Biosensors and Bioelectronics 87 (2017) 693–700

Contents lists available at ScienceDirect

Biosensors and Bioelectronics

journal homepage: www.elsevier.com/locate/bios

L-cysteine capped ZnS:Mn quantum dots for room-temperature detection of dopamine with high sensitivity and selectivity

Daysi Diaz-Diestra [a,b,c,*], Bibek Thapa [a,c,d], Juan Beltran-Huarac [a,d,*], Brad R. Weiner [a,b,c], Gerardo Morell [a,c,d]

[a] Molecular Sciences Research Center, University of Puerto Rico, San Juan, PR 00926, USA
[b] Department of Chemistry, University of Puerto Rico, San Juan, PR 00936, USA
[c] Institute for Functional Nanomaterials, University of Puerto Rico, San Juan, PR 00931, USA
[d] Department of Physics, University of Puerto Rico, San Juan, PR 00936, USA

ARTICLE INFO

Article history:
Received 8 July 2016
Received in revised form
5 September 2016
Accepted 6 September 2016
Available online 12 September 2016

Keywords:
Quantum dots
Dopamine
Mn-doped ZnS

ABSTRACT

Dopamine (DA) is one of the most important catecholamine neurotransmitters of the human central nervous system, and is involved in many behavioral responses and brain functions. Below normal DA levels in biological fluids can lead to different neurodegenerative conditions. For excess DA levels, a failure in energy metabolism is indicated. In this study, a facile room-temperature phosphorescence sensor is developed to detect DA based on L-cysteine capped Mn doped ZnS quantum dots (L-cys ZnS:Mn QDs). The QDs display a prominent orange emission band peaking at ~598 nm, which is strongly quenched upon addition of DA in alkaline medium. The sensor exhibits a linear working range of ~0.15–3.00 μM, and a limit of detection of ~7.80 nM. These results are explained in terms of a pH-dependent electron transfer process, in which the oxidized dopamine quinone functions as an efficient electron acceptor. The QDs-based sensor shows a high selectivity to DA over common interfering biomolecules (including some amino acids, ascorbic acid, chloride and glucose). The sensor has been successfully applied for the detection of DA in urine samples, yielding recoveries as high as 93%. Our findings indicate that our developed sensor exhibits high sensitivity and reproducibility to determine DA even in biological fluids where DA is at low levels, e.g., in the central nervous system, which is the usual clinical profile of a neurodegenerative disorder associated to the Parkinson's disease.

1. Introduction

The US National Institute of Neurological Disorders classifies Parkinson's disease as the second most common neurodegenerative disorder, affecting approximately one million people in the US (Yao et al., 2013). This disease is related to the loss of brain cells that produce dopamine (DA). DA is one of the most important catecholamine neurotransmitters of the human central nervous system, and is involved in many behavioral responses and brain functions (Mu et al., 2014). The normal levels of DA vary depending on its location in the nervous system, and fall within the range of 1–50 nM in the brain extracellular fluid. Abnormal levels of DA have been associated to several diseases. For instance, schizophrenia and aprosexia can result from deficient levels of DA, while pleasurable/rewarding feelings (even euphoria) and failure in energy metabolism are observed when DA is in excess (Hyman et al., 2001; Mu et al., 2014; Tobler et al., 2005). This makes the selective and sensitive detection of DA of paramount importance in health clinics and the pharmaceutical industry. Among the most used techniques to detect DA are colorimetry, chemiluminescence, gas and liquid chromatography, and electrochemical approaches (Alarcon-Angeles et al., 2008; Naccarato et al., 2014; Li et al., 2011a; Su et al., 2012; Ye et al., 2005). Nonetheless, there exist some limiting factors (including long operation times, overlapping signals, cumbersome methods of extraction, and interference from other biological molecules) that hinder their performance (Ban et al., 2015). To surmount these difficulties, room temperature (RT) fluorescence has been recently proposed due to its high sensitivity, detection reliability, safe manipulation, operational simplicity, real-time detection, and cost-effectiveness (Zhang et al., 2015a). The detection process of this spectroscopic technique is based on the effective interaction between the target analytes (such as metal ions and biomolecules) and fluorescent probes, which

* Corresponding authors at: Molecular Sciences Research Center, University of Puerto Rico, San Juan, PR 00926, USA.
E-mail addresses: daysi.diaz@upr.edu (D. Diaz-Diestra), juan.beltran1@upr.edu (J. Beltran-Huarac).

http://dx.doi.org/10.1016/j.bios.2016.09.022

induces energy transfer and in turn a detectable signal.

Quantum dots (QDs) used as fluorescent probes in chemo/biosensing offer significant advantages over organic molecules, genetically-encoded fluorophores and conventional dyes, in terms of simultaneously detecting multiple signals, producing long-term stabilities, and enriching both the biological targeting efficiency and substrate specificity (Alivisatos, 1996; Diaz-Diestra et al., 2015; Liao et al., 2014). In particular, Mn-doped ZnS (ZnS: Mn) QDs with intrinsic solubility in water have appeared as a potential fluorescent probe since they exhibit high resistance to photobleaching, broad absorption with relatively-narrow and symmetric emission, high quantum yield, and strong resistance to degradation. Their main features are not only analogous to those observed in Cd (Se, Te) QDs (most used as standards), but also ZnS:Mn QDs are non-toxic in a wide range of concentrations (Diaz-Diestra et al., 2015; Li et al., 2011b; Sotelo-Gonzalez et al., 2013; Zhang et al., 2011). In addition, the Mn-doping into the ZnS host further advances multiplicity of decay times, flexible bioconjugation approaches, enhanced surface passivation, large-effective Stokes shifts, intermittency under continuous excitation, and optical tunability (Diaz-Diestra et al., 2015; Liu et al., 2008a; Quan et al., 2009). Thus, ZnS:Mn can serve as a promising fluorescent nanoplatform with advantages over traditional detection systems. Its optical sensing is based on the interaction of a fraction of atoms/molecules on a treated surface, which strongly affects the recombination of electrons and holes within the particles, and in turn the emission response (Mu et al., 2014). Following this process, many analytes have been successfully detected, such as ions (Hg^{2+}, Co^{2+}, Zn^{2+} and Zr^{4+}) (Bian et al., 2014; Gong et al., 2014a; Ren et al., 2011; Tan et al., 2012); proteins/enzymes, clenbuterol and glucose in biological fluids (Gong et al., 2014b; Wu et al., 2013; Wu et al., 2010; Zhang et al., 2013); organophosphorus pesticides (Ban et al., 2014); phenols in different media (Liu et al., 2010; Wei et al., 2015; Zhang et al., 2015b); and cathecol, domoic acid, rutin, urea, idarubicin and DNA (Bi et al., 2014; Dan et al., 2013; Ertas et al., 2015; Miao et al., 2014; Wang et al., 2013). Recently, Bian and co-workers, employing N-acetyl-L-cysteine and L-cysteine capped ZnS:Mn QDs as probes, showed the luminescent detection of L-ascorbic acid (AA) with high selectivity and long luminescence lifetime (Bian et al., 2013). The authors exploited the fact that the RT luminescent intensity of the Mn-emission band is efficiently quenched by AA, which is converted into dehydro-AA via oxidation when exposed to Mn^{3+} ions. The ZnS:Mn optical sensor exhibited a linear working range of 2.5–47.5 μM with limits of detection (LOD) from 0.72 to 1.38 μM (Bian et al., 2013). Similarly, Zhang and co-workers modified the surface of ZnS:Mn nanocrystals with DA dithiocarbamate to detect diethylphosphorothioate (DEP) (Zhang et al., 2014). Modulating the dual emission of ZnS:Mn probe through a photo-induced electron transfer process, the authors enhanced the red emission by switching off the electron transfer pathway and keeping the blue emission almost unaltered. They obtained a linear response for DEP concentrations with a LOD of 1.8 μM (Zhang et al., 2014). However, even though the manganese energy levels in surface-modified ZnS:Mn QDs can facilitate the detection of certain analytes, the quenching effect of DA on the Mn-emission band of ZnS:Mn has not been studied. In addition, the interaction mechanism of DA with other QDs is still unclear to date.

Over the past few years, the interaction of DA with QDs has been assessed in bioconjugates and expressed in terms of redox interactions, in which DA quinone acts as an electron donor that quenches or sensitizes the QDs via a reactive oxygen-mediated mechanism (Clarke et al., 2006). It has been also reported that such bioconjugates function as charge-transfer coupled pH sensors, wherein DA is characterized by both the Nernstian dependence of formal potential on pH, and the oxidation of hydroquinone to quinone by O_2 at basic pH (Medintz et al., 2010). This signifies that the oxidized DA acts as an electron acceptor that quenches the QDs emission depending directly on pH. More recently, Qin and co-workers showed that the QDs-DA interactions could modulate the fluorescence and photoresponse of the DA-arginine-glycine-aspartic-acid-cysteine QDs system by specific trypsin activity (Qin et al., 2014). The authors reported that the fluorescence signal significantly increased as a result of the enzymatic cleavage of the active molecules, and that the photocurrent was enhanced as the trypsin concentration increased from 0 to 15 μg mL^{-1} (Qin et al., 2014). Mu and co-workers built a DA fluorescent sensor based on adenosine-capped CdSe/CdS/ZnS QDs, and found a LOD of ~20 nM with a linear working range of 100 nM to 20 μM, which was ascribed to the strong interaction between adenosine and DA (Mu et al., 2014). In parallel, Xiangzhao and co-workers reported that the silica-capped CdTe based sensor can detect DA in the range of 500 nM to 100 μM with a LOD of ~240 nM, which was associated to the hydrogen bonding and electrostatic interaction between silica and DA in alkaline solution (Xiangzhao et al., 2013). Although the interaction of DA with Cd-based QDs in the form of bioconjugates has been studied under certain conditions, the selective capture of DA molecules by surface-complexed ZnS:Mn QDs via a phosphorescent quenching process is still a big challenge. In this paper, we report for the first time the development of a room-temperature phosphorescence sensor based on L-cysteine (L-cys) capped ZnS:Mn QDs synthesized via a facile wet chemical approach, to detect DA in a wide range of concentrations (nM-μM). The advantage of using L-cysteine (a natural thiol-containing amino acid with excellent water solubility) is the fact that it endows L-cys capped ZnS:Mn QDs with further biocompatibility and great potential for room temperature detection of water-soluble analytes (such as dopamine) in biological fluids. In order to make our sensor more selective, we evaluate the discrimination of the DA detection from seven interfering analytes. Finally, we examine the accuracy of our method in real samples to determine DA in urine samples via a recovery test.

2. Experimental section

2.1. Synthesis of L-cysteine capped ZnS:Mn quantum dots

ZnS:Mn QDs capped with L-cysteine ($C_3H_7NO_2S$, ≥ 98.5%, Sigma Aldrich, USA) were prepared by an inorganic wet chemical approach, following our previous synthetic methodology (Diaz-Diestra et al., 2015) with some modifications. Briefly, 90 mg of $ZnSO_4 \cdot H_2O$ (≥ 99.9%, Sigma Aldrich, USA), 3.0 mg of $MnCl_2$ (≥ 99%, Sigma Aldrich, USA) and 121 mg of L-cysteine were dissolved into a 25 mL three-neck round-bottom flask using high-purity deionized water (HPDW), resulting in a 5 wt% Mn doping. The pH of the mixed solution was adjusted to 11 using 1 M NaOH (99.99%, Sigma Aldrich, USA). After purging with argon, 5 mL of 0.2 M aqueous solution of Na_2S (Sigma Aldrich, USA) was gradually added. The mixture was stirred under controlled reflux for 14 h at 50 °C in open air. The flocculate was removed from the supernatant by ultracentrifugation, and copiously rinsed with HPDW, and then freeze-dried. The final products were re-dispersed in HPDW and produced a deep orange solution when exposed to UV light. This orange color is a clear indicator of the compound formation, and is used for *ex-situ* characterization throughout the experiments.

2.2. Apparatus

The optical absorption spectra were recorded using a UV–vis spectrophotometer (DU 800, Beckman Coulter). A Cary Eclipse Spectrophotometer was employed to collect the emission spectra

in phosphorescence mode. The emission spectra were recorded from 400 to 700 nm, using slit widths of 10 and 20 nm for emission and excitation, respectively. The phase and crystalline structures of the QDs were analyzed using an X-Ray Diffractometer (XRD), Rigaku Smart-Lab Japan, equipped with a Cu Kα radiation source, and operated at an accelerating potential of 40 kV and a tube current of 44 mA. The FT-IR spectra were recorded using a Bruker Tensor 27 in the range of 100–4000 cm^{-1}. The surface morphology and crystallite size distribution were studied using a JEOL JEM-2200FS Cs-corrected high-resolution transmission electron microscope (HRTEM) operated at 200 kV.

2.3. Phosphorescence quenching of L-cysteine capped ZnS:Mn quantum dots by dopamine and discrimination of interfering analytes

In separate assays, L-cys capped ZnS:Mn QDs (300 μL, pH 7.0) and DA (0–3000 nM) were placed into 5 mL tubes. The mixtures were then diluted up to 3 mL using 10 mM PBS (pH 8.0) and mixed thoroughly. Afterwards, the pH of the final solutions were optimized (from 5.0 to 8.5) using 1 M NaOH, and were then excited with 302 nm light to collect the emission spectra at different times (0–60 min). A similar procedure was followed for discriminating DA from seven interfering analytes (KCl, L-histidine, dihydroxyphenylacetic acid, L-glutamine, L-glucose, L-aspartic acid and ascorbic acid (AA) at 10 μM). All the experiments were repeated in triplicate and performed at RT.

2.4. Detection of dopamine in real samples

In order to detect DA in biological fluids, urine samples were subjected to a 100-fold dilution process using a 10 mM PBS solution (pH 8.0) before analyses. In a typical assay, different concentrations (5–1000 nM) of DA and L-cysteine capped ZnS:Mn QDs (300 μL, pH 7.0) were mixed with diluted urine. Then, this mixture was added to a solution consisting of 20 μL DA and PBS obtaining a final volume of 3 mL at pH 8.0. The as-prepared samples were excited with 302-nm light to collect the emission spectra after 30 min. All the experiments were repeated in triplicate and performed at RT.

3. Results and discussion

3.1. Characterization of L-cysteine capped ZnS:Mn quantum dots

The surface morphology and particle size distribution of the products synthesized via a one-pot wet chemical approach are depicted in Fig. 1. The HRTEM image displayed in Fig. 1a shows thin clusters consisting of particles with high definition. A closer look indicates that the particles are near-spherical and homogeneously distributed with a high degree of crystallinity, whose sizes range from 1 to 5 nm (see Fig. 1b). From the gray scale contrasts, the nanoparticles appear to be composed of another extra amorphous phase, which is ascribed to the capping layer. The statistical size distribution obtained by image analysis further confirmed that the size of nanoparticles falls in the range of 1–5 nm, with an average particle size of ~2.8 nm (see inset of Fig. 1b). This analysis points out that the nanoparticles are monodispersed. To assess the nanoparticles' phase, we carried out selective area electron diffraction (SAED) on the region shown in Fig. 1a. The SAED pattern depicted in the inset of Fig. 1a shows three major diffraction rings, which are indexed to the diffraction planes of the cubic sphalerite phase of polycrystalline ZnS [(111), (220) and (311)] according to the JCPDS card, File No. 65–0309 (Diaz-Diestra et al., 2015).

To further confirm the preferential cubic crystallization, we conducted X-ray diffraction on bulk samples. The XRD pattern shows three diffraction peaks, which are indexed to the diffraction planes of stable cubic ZnS (see Fig. S1a). The prominent broadening of the XRD diffraction peaks is ascribed to the nanocrystalline nature of ZnS: Mn. No detectable shifts (lattice distortion) of the diffraction peaks were observed, which is indicative of the successful random substitution of Mn^{2+} into Zn^{2+} sites at 5 wt% Mn doping. The average crystallite size was calculated to be ~2.1 nm by means of Scherrer's formula, in agreement with the image analysis. Taken altogether, both diffraction techniques and electron microscopy provide evidence that ZnS:Mn nanoparticles are free of both parasitic phases and hexagonal ZnS traces, and they are of high crystalline quality and purity.

To verify the bonding of L-cysteine capping ligand onto the nanoparticles surface, we conducted an FTIR analysis. The FT-IR spectra of the L-cys capped ZnS:Mn and L-cysteine are depicted in Fig. S1b. It is noteworthy that in our synthetic methodology the pH

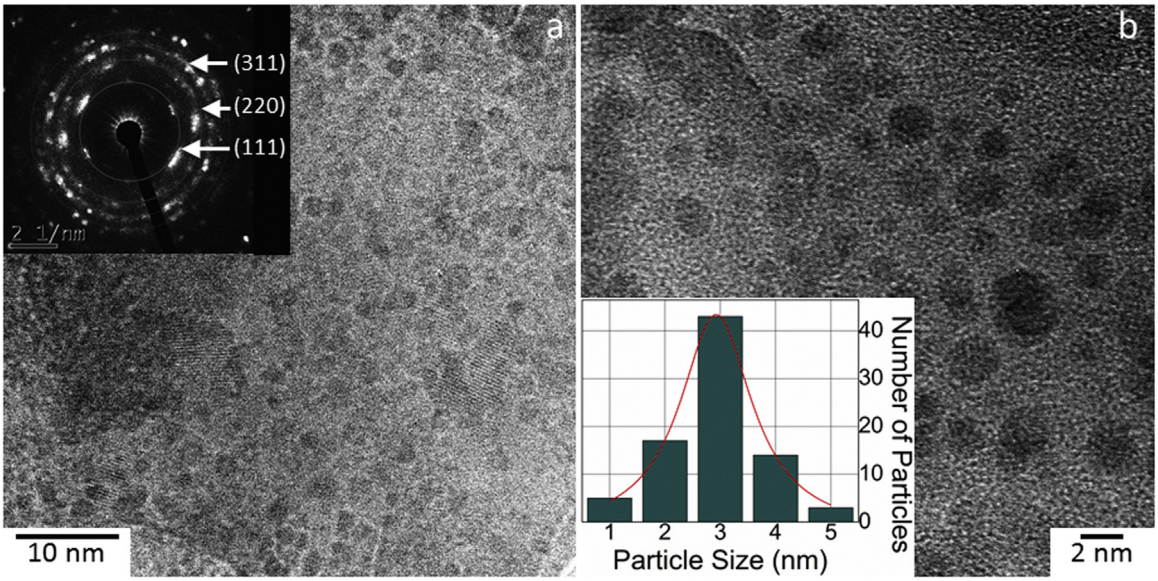

Fig. 1. Bright-field HRTEM images (a, b) of L-cys capped ZnS:Mn QDs. The insets in (a) and (b) show the SAED rings and particle size distribution of L-cys capped ZnS:Mn QDs.

level was adjusted to 11 in order to deprotonate the carboxylic end of the L-cysteine, and in turn to reinforce the bonding. The FT-IR spectrum of bare L-cysteine shows a pronounced band at ~2600 cm^{-1}, which is ascribed to the typical S-H stretching of L-cysteine (Bian et al., 2013). It was found that this band vanishes when L-cysteine is linked onto the ZnS:Mn surface, indicating the successful formation of S–Zn and S-Mn bonds between the ligand and nanoparticles. The FT-IR spectrum of L-cys capped ZnS:Mn shows three main absorption bands at ~3500–3000 cm^{-1} (m_ν OH, COOH), ~1550–1600 cm^{-1} (s_ν COO^-) and ~1400 cm^{-1} (m_ν COO^-), and one absorption band at ~2900–3420 cm^{-1}, which correspond to the carboxylic functionality and the amino group, respectively. This observation confirms that L-cysteine has been successfully attached on the ZnS:Mn surface, and that an effective deprotonation process of L-cysteine was achieved, which is evidenced by the presence of the carboxylate moieties.

The optical properties of L-cys ZnS:Mn nanoparticles in aqueous media were studied via UV–vis spectroscopy. The absorption and emission spectra of L-cys ZnS:Mn nanoparticles are depicted in Fig. S2. The UV–vis spectrum shows a broad band that reaches a maximum absorption at ~297 nm, which is attributed to the exciton transition of ZnS (Augustine et al., 2013). This represents a blue shift of ~40 nm when compared to bulk ZnS, which is attributed to the quantum confinement effect since the average crystallite size is comparable to the exciton Bohr radius (~2.5 nm) (Augustine et al., 2013). The same spectral position of this band was observed for both ZnS and ZnS:Mn QDs, as expected. The phosphorescent spectrum shows a prominent orange emission band at ~598 nm, which is associated to the internal Mn^{2+} ion transition between the $^4T_1$ first excited state (spin 3/2) and the $^6A_1$ ground state (spin 5/2) (Beltran-Huarac et al., 2013). Note that the blue band at ~416 nm (ascribed to the nanostructure surface states) typically observed in dual-emitting ZnS:Mn QDs was not detected by the spectrometer since it was operated in phosphorescence mode (Ertas et al., 2015) The blue band of the QDs when the spectrometer is operated in fluorescence mode was reported in our previous work (Diaz-Diestra et al., 2015). The internal transition is assumed to cause energy transfer from *s-p* electron-hole pair band states (host ZnS nanocrystal) to the Mn^{2+} ion *d*-electron states. These results confirm that the incorporation of Mn^{2+} ions into the ZnS host was homogeneous.

3.2. Effect of the reaction time and pH on the detection of dopamine

Although the prepared L-cysteine capped ZnS:Mn QDs is stable in water without visible precipitation after long aging times (few days), the orange emission band is observed to change as a function of time and pH. For this reason, the luminescent quenching effect of the QDs-based sensor is better monitored in phosphate buffer (PBS) for biological applications. The quenching of L-cys capped ZnS:Mn QDs luminescence by DA was studied in PBS media and used to quantify the DA detection. In order to detect DA with high sensitivity, the interaction time between DA molecules and L-cys capped QDs, and the pH dependence were first optimized. A linear relationship between the luminescence intensity and the concentration of the QDs over a wide range of concentrations, as previously reported, was observed (Ban et al., 2015). The concentration of the sensing probe was idealized to be ~55 mM, which provides a stable and detectable luminescence signal and avoids oversaturation. This concentration, which is compatible with that reported to detect other analytes (Bian et al., 2013), was used for further analysis. The effect of the reaction time (0–60 min) on the emission intensity of L-cys capped ZnS:Mn QDs in the presence of 0.8 μM DA is depicted in Fig. 2a. We observed that as time increases the luminescence intensity gradually decreases, which is attributed to the interaction between the DA target and L-cys ZnS:Mn probe via a charge transfer mechanism (Medintz et al., 2010). Fig. 2a also shows that the luminescent intensity is linear in the range of 0–60 min. We have thus taken the mean value (30 min) as suitable for the pH-dependent studies. Although the quenching apparently starts going slow, for instance in the interaction of DA and nanoclusters (Ban et al., 2015), our observations indicate that the interaction between DA and ZnS:Mn takes longer times until reaching the quenching saturation, which is related to the proper L-cysteine linkage (Qin et al., 2014).

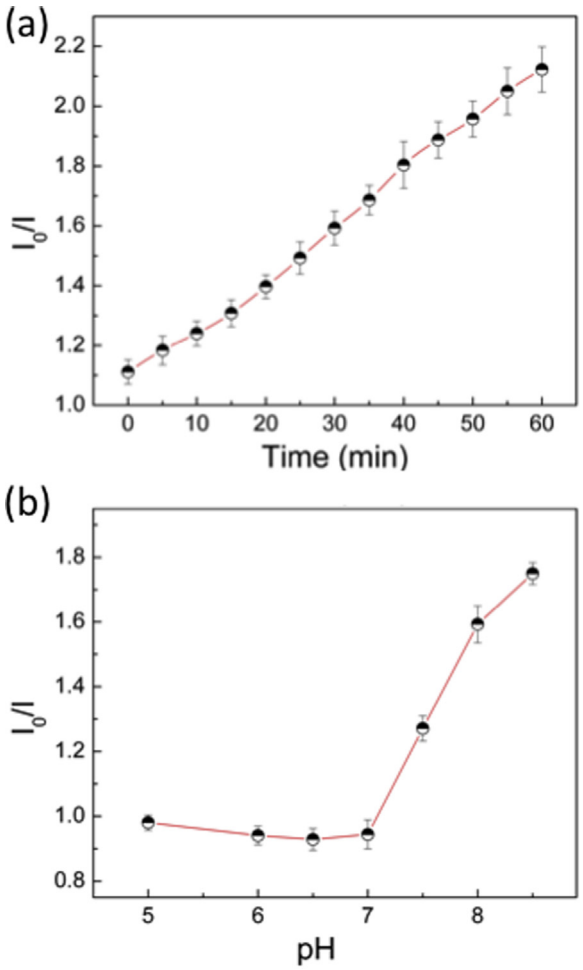

Fig. 2. The effect of the interaction time (a) and pH (b) on the emission intensity of L-cys capped ZnS:Mn QDs in the presence of DA.

The effect of pH (5.0–8.5) on the emission intensity of L-cys capped ZnS:Mn QDs in the presence of 0.8 μM DA is depicted in Fig. 2b. It was found that the luminescence intensity remains essentially the same in the range of 5.0–7.0, and then gradually decreases above 7.0 up to a pH value of 8.0. This is due to the fact that at high pH values, DA is rapidly oxidized to its quinone derivative, causing in turn an effective reactive quenching of L-cys capped ZnS:Mn QDs. We observed that the luminescence intensity and the stability of L-cys capped ZnS:Mn QDs is reduced at pH values higher than 8.5. This instability could be related to the offset of the noncovalent binding (caused by the electrostatic repulsion between the DA anions and the electronegative parts of L-cys capped QDs), which repels the rebinding of DA. We thereby set the pH to 8.0 as a tradeoff to minimize the DA repulsion and partial autopolymerization of the unstable quinone derivative, and the subsequent formation of polydopamine (Ban et al., 2015; Yildirim et al., 2014; Zhou et al., 2015). The luminescence quenching effect was further analyzed at this pH for 30 min

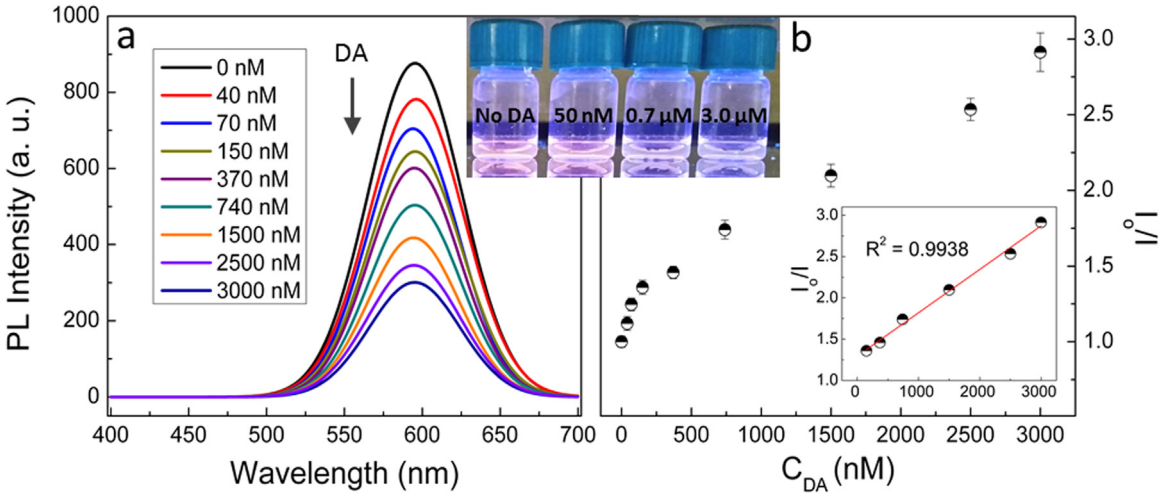

Fig. 3. Phosphorescence emission spectra (a) of L-cys capped ZnS:Mn QDs in the presence of different concentrations of DA (0–3000 nM). Stern-Volmer plots of I_o/I as a function of the DA concentration (0–3000 nM) (b). Lower inset shows the expanded linear region of the calibration curve. Upper inset shows the optical images of the phosphorescence quenching that undergoes the QDs as DA concentration increases (excitation light: 302 nm).

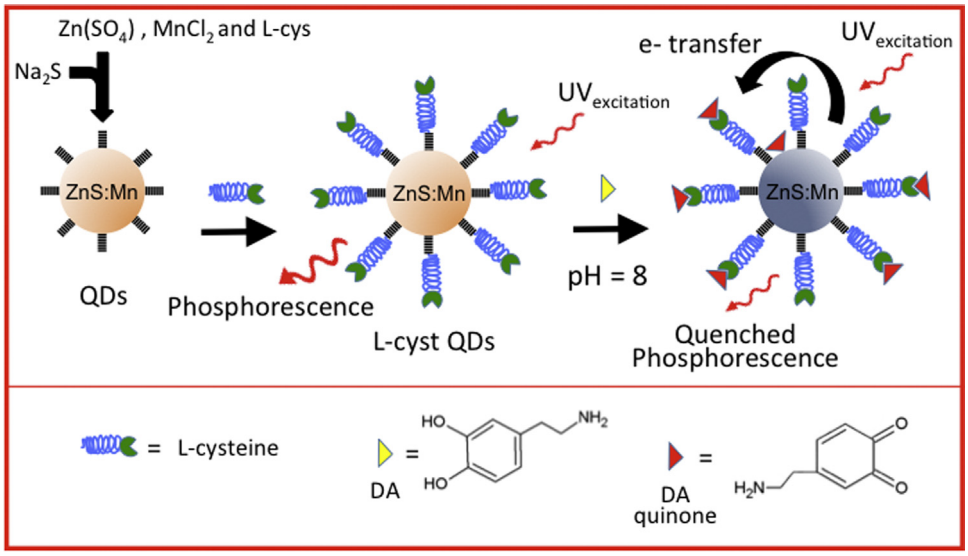

Scheme 1. Depiction illustrating the sensor design and selective dopamine detection through a phosphorescence quenching mechanism.

3.3. *Effect of the concentration of dopamine on the phosphorescence quenching*

The quenching ability of dopamine on the phosphorescence emission of L-cys capped ZnS:Mn QDs was recorded by adding various DA concentrations to the solution (see Fig. 3a). It was observed that the intensities decrease as the DA concentration increases from 0 to 3000 nM (see upper inset). No additional, detectable change in the spectral shape was seen, as expected. Fig. 3b shows the Stern-Volmer plots of I_0/I as a function of the DA concentration from 0 to 3000 nM, where I_0 and I are the emission intensities at 598 nm in the absence and presence of DA, respectively. A linear response was observed in the range of 150–3000 nM with a correlation coefficient of 0.9938 (see lower inset). The fitting curve generated a linear equation: $I_0 - I = 248.33 + 0.11$ [DA]. Using six replicate detections of DA, we determined the limit of detection (LOD) (Chandran et al., 2006) to be ~7.80 nM, which indicates that L-cys ZnS:Mn QDs possesses high sensitivity to detect DA. This value is 1–2 orders of magnitude higher than those reported for Cd-based QDs probes for detection of DA via fluorescence and electro-generated chemiluminescence methods (Mu et al., 2014; Liu et al., 2008b; Xiangzhao et al., 2013).

Although the concentration of DA varies depending on its location in the nervous system, it has been consistently reported that DA concentration is at the nanomolar scale, falling within the range of 1–50 nM in the brain extracellular fluid (O'neill, 1994). Our sensor is thus sensitive enough to detect DA in this biological setting, especially when DA concentrations are low, e.g., in the central nervous system. This situation represents the usual clinical profile of a neurodegenerative disorder associated to Parkinson's disease (Yao et al., 2013), in which a major loss (> 80%) of dopaminergic neurons (responsible for DA production) is manifested (Spina et al., 1989). Based on these observations, we assume that the DA detection arises from a phosphorescent quenching process, which can be accounted for in terms of a pH dependent electron transfer from the QDs to oxidized dopamine quinone. Under alkaline conditions and ambient O_2 exposure, dopamine oxidizes forming dopamine quinone, which is absorbed onto the QDs strongly interacting with the L-cysteine shell anchored to the QDs surface via non-covalent interactions, such as hydrogen bonding (O-H) and electrostatic interactions. Then, in parallel, the photo-excited electrons in the conduction band undergo intersystem crossing to the $^4T_1$ first excited state of Mn (see emission analysis), followed by transfer to the lowest unoccupied molecular orbital of

the dopamine quinone resulting in phosphorescence quenching. A summarized illustration is depicted in Scheme 1. It is well known that under alkaline conditions and exposure of solution-containing O_2, dopamine quinone acts an efficient electron acceptor and is kept at a short distance from the donor (QDs) (Laviron et al., 1984; Medintz et al., 2010; Wraight et al., 2004). This would explain why electrons are captured instead of recombining in the $^6A_1$ ground state of Mn, thus favoring an electron transfer rather than a recombination process at the interface of the QDs. This mechanism was further validated to explain the detection of DA using.

adenosine, β-cyclodextrin and trimethoxysilane-capped nanostructures as fluorescent probes (Ban et al., 2015; Mu et al., 2014; Zhang et al., 2015a). Accordingly, we assume that L-cys ZnS:Mn is mimicking the function of receptor proteins of the neurons during synapse by receiving the DA (at nanomolar range) from axon terminals, thus enabling the passage of chemical/electrical signals to other neurons.

3.4. Effect of other biomolecules

Besides the sensitivity requirement, high selectivity is a crucial matter to be met in real sensors to detect DA, especially when interfering substances co-exist within the biological samples. To verify the selectivity of the L-cys ZnS:Mn QDs probe for DA detection, the phosphorescent signals from common interfering analytes including KCl, L-histidine, dihydroxyphenylacetic acid, L-glutamine, L-glucose, L-aspartic acid and AA, were investigated and compared to that of DA (see Fig. 4). In order to highlight the high selectivity of our QDs-based sensor, we used concentrations two orders of magnitude higher than that of the DA (interfering analytes 10 μM and DA 0.2 μM). Fig. 4 shows a pronounced selective quenching by DA over the other biomolecules, i.e. ~1.6-fold less intense than the intensity drop produced by AA, the most competitive interferent in the determination of DA. AA is found in excess (compared to DA) in the extracellular fluid of the central nervous system, where both co-exist (Ali et al., 2007). The fact that AA does not affect significantly the phosphorescence intensity of the probe is likely due to its low binding constant with L-cysteine (Ankireddy et al., 2015; Ban et al., 2015), and this result can be used to determine DA concentrations without further sample separation. The weak interference in detecting the 200-nM concentration of DA in the presence of the other surrounding amino acids, glucose and chloride shows the strong non-covalent interaction between DA and L-cys ZnS: Mn, even when the more electronegative parts might repel the immersed analytes. Our findings indicate that our proposed assay exhibits high selectivity

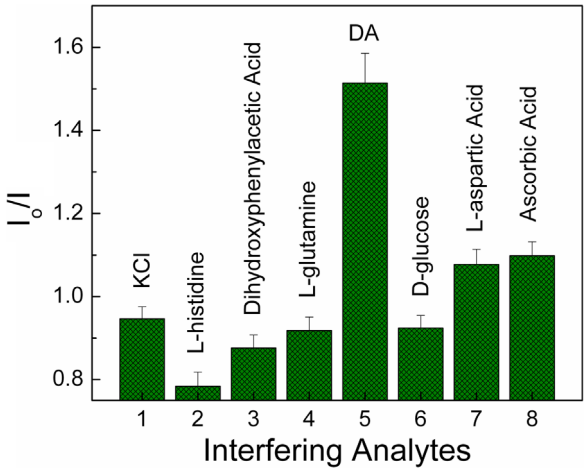

Fig. 4. Relative photoluminescence response of L-cys capped ZnS:Mn QDs probe in the presence of 200 nM DA and other interfering analytes (10 μM).

Table 1
Recovery test for the detection of DA in urine samples (n=3).

Sample	Added concentration (nM)	Found by our method (nM)	Recovery (%)	RSD (%)
1	5.0	6.3	80	2.1
2	150.0	143.9	96	1.3
3	1000.0	933.0	93	6.2

and could be used to detect DA in biological samples.

3.5. Effect of the medium

After corroborating the sensitivity and selectivity of ZnS:Mn QDs phosphorescent probes to detect DA, we evaluated its performance in a biological medium, which exhibits significant autophosphorescence background but negligible room-temperature phosphorescence (Wang et al., 2013). Thus, the possibility of investigating a real application applying our method to determine DA in urine was explored. Urine samples were subjected to a 100-fold dilution process using a 10 mM PBS solution (pH 8.0) before analyses, and the determination of DA was found using a similar calibration curve shown in Fig. 3. Table 1 summarizes the recovery tests for the detection of DA in urine samples of three concentrations (low, intermediate and high) for our method, which was compared to the method of reference (from the average of three replicate determinations). Our results show that the recovery and RSD values are in the range of 80–93% and 1.3–6.2%, respectively, and show high consistency when both methods are compared. RSD $<6.2\%$ indicates that the sensor shows good reproducibility. Since urine is mainly composed of amino acids, glucose and anions/cations, our recovery results further confirm that these co-existing biomolecules do not significantly interfere with the DA detection in diluted urine samples. Using this approach, similar results were reported to detect AA, vanillin, cyanide ions and organophosphate in urine, food, tap/ground and lake water, respectively (Bian et al., 2013; Duran et al., 2015; Shamsipur et al., 2014; Zhang et al., 2014). Finally, our findings reveal the potential applicability and accuracy of our ZnS:Mn phosphorescent probes to detect DA in biological fluids with high sensitivity and selectivity.

4. Conclusions

We have successfully developed a cost-effective room-temperature phosphorescence sensor to detect DA based on L-cys capped ZnS:Mn QDs. Our sensor is highly sensitive at the nanomolar range (LOD ~8 nM), which is 1–2 orders of magnitude higher than those reported by other techniques, including fluorescence and electro-generated chemiluminescence. We have observed that the phosphorescence of the QDs is only slightly quenched by AA and other interfering analytes (that coexist with DA), even at concentrations two orders of magnitude higher that of the DA, signifying that our sensor is highly selective. The fact that AA does not significantly affect the phosphorescence intensity was ascribed to its low binding constant with L-cysteine, which can be exploited in clinical trials to determine DA without resorting to complex and additional separation processes to analyze samples. We have also shown that our method can be applied to determine DA in urine or other body fluids that are mainly composed of amino acids, glucose and anions/cations. For urine, we found recovery values as high as 93% with a low relative standard deviation. Our detection approach based on phosphorescence signals offers a remarkable advantage since biological fluids do not

show significant phosphorescence response, resulting in a high signal-to-noise ratio. Besides measuring the concentration of DA in urine samples, this piece of research represents a step forward in the development of water-soluble phosphorescent probes, which could be used for imaging neurodegenerative disorders in the central nervous system, such as the Parkinson's disease.

Acknowledgements

This project was partially supported by the Institute for Functional Nanomaterials (NSF Grant 1002410) and PR NASA EPSCoR (NASA Cooperative Agreement NNX13AB22A). Authors thank the valuable assistance of Mr. Oscar Resto for providing the HRTEM images.

Appendix A. Supplementary material

Supplementary data associated with this article can be found in the online version at http://dx.doi.org/10.1016/j.bios.2016.09.022.

References

Alarcon-Angeles, G., Perez-Lopez, B., Palomar-Pardave, M., Ramirez-Silva, M.T., Alegret, S., Merkoçi, A., 2008. Enhanced host–guest electrochemical recognition of dopamine using cyclodextrin in the presence of carbon nanotubes. Carbon 46, 898–906.
Ali, S.R., Parajuli, R.R., Ma, Y., Balogun, Y., He, H., 2007. Interference of ascorbic acid in the sensitive detection of dopamine by a nonoxidative sensin approach. J. Phys. Chem. B 111, 12275–12281.
Alivisatos, A.P., 1996. Semiconductor clusters, nanocrystals, and quantum dots. Science 271, 933–937.
Ankireddy, S.R., Kim, J., 2015. Selective detection of dopamine in the presence of ascorbic acid via fluorescence quenching of InP/ZnS quantum dots. Int. J. Nanomed. 10, 113–119.
Augustine, M.S., Ali, P.P.M., Sapna, K., Elyas, K.K., Jayalekshmi, S., 2013. Size dependent optical properties of bio-compatible ZnS:Mn nanocrystals and their application in the immobilization of trypsin. Spectrochim. Acta, Part A 108, 223 228.
Ban, R., Zhu, J.-J., Zhang, J., 2014. Manganese-doped ZnS quantum dots as a phosphorescent probe for use in the bi-enzymatic determination of organophosphorus pesticides. Microchim. Acta 181, 1591–1599.
Ban, R., Abdel-Halim, E.S., Zhang, J., Zhu, J.-J., 2015. β-cyclodextrin functionalised gold nanoclusters as luminescence probes for the ultrasensitive detection of dopamine. Analyst 140, 1046–1053.
Beltran-Huarac, J., Wang, J., Tanaka, H., Jadwisienczak, W.M., Weiner, B.R., Morell, G., 2013. Stability of the Mn photoluminescence in bifunctional ZnS:0.05Mn nanoparticles. J. Appl. Phys. 114, 053106.
Bi, L., Dong, X.-T., Yu, Y.-H., 2014. Room temperature phosphorescence sensor based on manganese doped zinc sulfide quantum dots for detection of urea. J. Lumin. 153, 356–360.
Bian, W., Ma, J., Liu, Q., Wei, Y., Li, Y., Dong, C., Shuang, S., 2014. A novel phosphorescence sensor for Co^{2+} ion based on Mn-doped ZnS quantum dots. Luminescence 29, 151–157.
Bian, W., Ma, J., Guo, W., Lu, D., Fan, M., Wei, Y., Li, Y., Shuang, S., Choi, M.M.F., 2013. phosphorescence detection of L-ascorbic acid with surface-attached N Acetyl-L-Cysteine and L-Cysteine Mn doped ZnS quantum dots. Talanta 116, 794–800.
Chandran, S., Singh, R.S.P., 2006. Comparison of various international guidelines for analytical method validation. Pharmazie 62, 4–14.
Clarke, S.J., Hollmann, A., Zhang, Z., Suffern, D., Bradforth, S.E., Dimitrijevic, N.M., Minarik, W.G., Nadeau, J.L., 2006. Photophysics of dopamine modified quantum dots and effects on biological systems. Nat. Mater. 5, 409–417.
Dan, L., Wang, H.-F., 2013. Mn-doped ZnS quantum dot imbedded two-fragment imprinting silica for enhanced room temperature phosphorecence probing of domoic acid. Anal. Chem. 85, 4844–4848.
Diaz-Diestra, D., Beltran-Huarac, J., Bracho-Rincon, D.P., González-Feliciano, J.A., Gonzalez, C.I., Weiner, B.R., Morell, G., 2015. Biocompatible ZnS:Mn quantum dots for reactive oxygen generation and detection in aqueous media. J. Nanopart. Res. 17, 461.
Duran, G.M., Contento, A.M., Rios, A., 2015. β–cyclodextrin coated CdSe/ZnS quantum dots for vanillin sensoring in food samples. Talanta 131, 286–291.
Ertas, N., Kara, H.E.S., 2015. L-cysteine capped Mn-doped ZnS quantum dots as a room temperature phosphorescence sensor for in-vitro binding assay of idarubicin and DNA. Biosens. Bioelectron. 70, 345–350.
Gong, Y., Fan, Z., 2014a. Highly selective manganese-doped zinc sulfide quantum dots based label free phosphorescent sensor for phosphopeptides in presence of Zirconium (IV). Biosens. Bioelectron. 66, 533–538.
Gong, Y., Fan, Z., 2014b. Melamine-modulated mercaptopropionic acid-capped manganese doped zinc sulfide quantum dots as a room-temperature phosphorescence sensor foe detecting clenbuterol in biological fluids. Sens. Actuators, B 202, 638–644.
Hyman, S.E., Malenka, R.C., 2001. Addiction and the brain: the neurobiology of compulsion and its persistence. Nat. Rev. Neurosci. 2, 695–703.
Laviron, E., 1984. Electrochemical reactions with protonations at equilibrium. the kinetics of the parabenzoquinone hydroquinone couple on a platinum electrode. J. Electroanal. Chem. 164, 213–227.
Li, H., Li, M., Shih, W.Y., Lelkes, P.I., Shih, W.H., 2011b. Cytotoxicity test water solule ZnS and CdS quantum dots. J. Nanosci. Nanotechnol. 11, 3543–3551.
Li, L., Liu, H., Shen, Y., Zhang, J., Zhu, J.-J., 2011a. Electrogenerated chemiluminescence of Au nanoclusters for the detection of dopamine. Anal. Chem. 83, 661–665.
Liao, Y., Zhou, X., Xing, D., 2014. Quantum dots and graphene oxide fluorescent switch based multivariate testing strategy for reliable detection of listeria monocytogenes. ACS Appl. Mater. Interfaces 6, 9988–9996.
Liu, J., Chen, H., Lin, Z., Lin, J.-M., 2010. Preparation of surface imprinting polymer capped Mn-doped ZnS quantum dots and their application for chemiluminescence detection of 4-nitrophenol in tap water. Anal. Chem. 82, 7380–7386.
Liu, X., Ni, X., Wang, J., Yu, X., 2008a. A novel route to photoluminescent, water soluble Mn-doped ZnS quantum dots via photopolymerization initiated by the quantum dots. Nanotechnology 19, 485602.
Liu, X., Cheng, L.X., Lei, J.P., Ju, H.X., 2008b. Dopamine detection based on its quenching effect on the anodic electrochemiluminescence of CdSe quantum dots. Analyst 133, 1161–1163.
Medintz, I.L., Stewart, M.H., Trammell, S.A., Susumu, K., Delehanty, J.B., Mei, B.C., Melinger, J.S., Blanco-Canosa, J.B., Dawson, P.E., Mattoussi, H., 2010. Quantum dot/dopamine bioconjugates function as redox coupled assemblies for in vitro and intracellular pH sensing. Nat. Mater. 9, 676–684.
Miao, Y., Zhang, Z., Gong, Y., Zhang, Q., Yan, G., 2014. Self-assembly of manganese doped zinc sulfide quantum dots/CTAB nanohybrids for detection of rutin. Biosens. Bioelectron. 52, 271–276.
Mu, Q., Xu, H., Li, Y., Ma, S., Zhong, X., 2014. Adenosine capped QDs based fluorescent sensor for detection of dopamine with high selectivity and sensitivity. Analyst 139, 93–98.
Naccarato, A., Gionfriddo, E., Sindona, G., Tagarelli, A., 2014. Development of a simple and rapid solid phase microextraction-gas chromatography-triple quadrupole mass spectrometry method for the analysis of dopamine, serotonin and norepinephrine in human urine. Anal. Chim. Acta 810, 17–24.
O'Neill, R.D., 1994. Microvoltammetric techniques and sensors for monitoring neurochemical dynamics in vivo. Analyst 119, 767–779.
Qin, L., Ji, C., He, L., Li, X., Kang, S., Mu, J., 2014. Interactions between quantum dots and dopamine coupled via a peptide bridge. RSC Adv. 4, 2143–2150.
Quan, Z., Yang, D., Li, C., Kong, D., Yang, P., Cheng, Z., Lin, J., 2009. Multicolor tuning of manganese-doped colloidal nanocrystals. Langmiur 25, 10259–10262.
Ren, H.-B., Wu, B.-Y., Chen, J.-T., Yan, X.-P., 2011. Silica-coated S^2—enriched manganese doped ZnS quantum dots as a photoluminescence probe for imaging intracellular Zn^{2+} ions. Anal. Chem. 83, 8239–8244.
Shamsipur, M., Rajabi, H.R., 2014. Pure zinc sulfide quantum dot as highly selective luminescent probe for determination of hazardous cyanide ion. Mater. Sci. Eng. C 36, 139–145.
Sotelo-Gonzalez, E., Roces, L., Garcia-Granda, S., Fernandez-Arguelles, M.T., Costa Fernandez, J.M., Sanz-Medel, A., 2013. Influence of Mn^{2+}-doped ZnS quantum dots synthesis: evaluation of the structural and photoluminescent properties. Nanoscale 5, 9156–9161.
Spina, M.B., Cohen, G., 1989. Dopamine turnover and glutathione oxidation: implications for parkinson disease. Proc. Natl. Acad. Sci. 86, 1398–1400.
Su, H., Sun, B., Chen, L., Xu, Z., Ai, S., 2012. Colorimetric sensing of dopamine based on the aggregation of gold nanoparticles induced by copper ions. Anal. Methods 4, 3981–3986.
Tan, L., Li, Y., Tang, Y., Kang, C., Yu, Z., Xu, S., 2012. Room temperature phosphorescence sensor for Hg2+ based on mn-doped ZnS quantum dots. J. Nanosci. Nanotechnol. 12, 7788–7795.
Tobler, P.N., Fiorillo, C.D., Schultz, W., 2005. Adaptive coding of reward value by dopamine neurons. Science 307, 1642–1645.
Wang, H.-F., Wu, Y.-Y., Yan, X.-P., 2013. Room-temperature phosphorescent discrimination of cathecol from resorcinol and hydroquinone based on sodium tripolyphosphate capped Mn-doped ZnS quantum dots. Anal. Chem. 85, 1920–1925.
Wei, X., Zhou, Z., Hao, T., Li, H., Yan, Y., 2015. Molecularly imprinted polymer nanospheres based on MN-doped ZnS QDs via precipitation polymerization for room temperature phosphorescence probing of 2,6 Dichlorophenol. RSC Adv. 5, 19799–19806.
Wraight, C.A., 2004. Proton and electron transfer in the acceptor quinone complex of photosynthetic reaction centers from rhodobacter sphaeroides. Front. Biosci. 9, 309–337.
Wu, P., He, Y., Wang, H.-F., Yan, X.-P., 2010. Conjugation of glucose oxidase onto Mn doped ZnS quantum dots for phosphorescent sensing of glucose in biological fluids. Anal. Chem. 82, 1427–1433.
Wu, P., Zhao, T., Tian, Y., Wu, L., Hou, X., 2013. Protein-directed synthesis of Mn doped ZnS quantum dots: a dual-channel biosensor for two proteins. Chem. Eur. J. 19, 7473–7479.
Xiangzhao, A., Qiang, M., Xingguang, S., 2013. Nanosensor for dopamine and glutathione based on the quenching and recovery of the fluorescence of silica

coated quantum dots. Microchim. Acta 180, 269–277.
Yao, S.C., Hart, A.D., Terzella, M.J., 2013. An evidence-based osteopathic approach to parkinson disease. Osteopath. Fam. Physician 3, 96–101.
Ye, X., Kuklenyik, Z., Needham, L.L., Calafat, A.M., 2005. Automated on-line column switching HPLC-MS/MS method with peak focusing for the determination of nine environmental phenols in urine. Anal. Chem. 77, 5407–5413.
Yildirim, A., Bayindir, M., 2014. Turn-on fluorescent dopamine sensing based on in situ formation of visible light emitting polydopamine nanoparticles. Anal. Chem. 86, 5508–5512.
Zhang, K., Yu, T., Liu, F., Sun, M., Yu, H., Liu, B., Zhang, Z., Jiang, H., Wang, S., 2014. Selective fluorescence turn-on and ratiometric detection of organophosphate using dual-emitting Mn-doped ZnS nanocrystal probe. Anal. Chem. 86, 11727–11733.
Zhang, L., Cui, P., Zhang, B.C., Gao, F., 2013. Aptamer-based turn-on detection of thrombin in biological fluids based on efficient phosphorescence energy transfer from Mn-doped ZnS quantum dots to carbon nanodots. Chem. Eur. J. 19, 9242–9250.
Zhang, W., Li, Y., Zhang, H., Zhou, X., Zhong, X., 2011. Facile synthesis of highly luminescent Mn-doped ZnS nanocrystals. Inorg. Chem. 50, 10432–10438.
Zhang, X., Yang, S., Zhao, W., Sun, L., Luo, A., 2015b. Mn-doped ZnS QDs entrapped in molecularly membranes for detection of trace bisphenol A. Anal. Methods 7, 8212–8219.
Zhang, X., Chen, X., Kai, S., Wang, H.-Y., Yang, J., Wu, F.-G., Chen, Z., 2015a. Highly sensitive and selective detection of dopamine using one-pot synthesized highly photoluminescent silicon nanoparticles. Anal. Chem. 87, 3360 3365.
Zhou, X., Wang, A., Yu, C., Wu, S., Shen, J., 2015. Facile synthesis of molecularly imprinted graphene quantum dots for the determination of dopamine with affinity adjustable. ACS Appl. Mater. Interfaces 7, 11741–11747.